

UCSF

UC San Francisco Previously Published Works

Title

Brain metabolism after therapeutic hypothermia for murine hypoxia-ischemia using hyperpolarized [1-13C] pyruvate magnetic resonance spectroscopy

Permalink

<https://escholarship.org/uc/item/15v7t5wn>

Journal

NMR in Biomedicine, 37(10)

ISSN

0952-3480

Authors

Liu, Xiaodan

Manninen, Tiina

Capper, Alkisti Mikrogeorgiou

et al.

Publication Date

2024-10-01


DOI

10.1002/nbm.5196

Peer reviewed

RESEARCH ARTICLE

Brain metabolism after therapeutic hypothermia for murine hypoxia-ischemia using hyperpolarized [1-¹³C] pyruvate magnetic resonance spectroscopy

Xiaodan Liu^{1,2}  | Tiina Manninen^{2,3} | Alkisti Mikrogeorgiou Capper² |
Xiangning Jiang² | Jacob Ellison^{1,4} | Yaewon Kim¹ | Gokce Gurler⁵ |
Duan Xu^{1,4} | Donna M. Ferriero²

¹Department of Radiology and Biomedical Imaging, University of California San Francisco, San Francisco, California, USA

²Department of Neurology, University of California San Francisco, San Francisco, California, USA

³Faculty of Medicine and Health Technology, Tampere University, Tampere, Finland

⁴Joint UCSF/UC Berkeley Graduate Group in Bioengineering, San Francisco, California, USA

⁵Faculty of Medicine, Hacettepe University, Ankara, Turkey

Correspondence

Duan Xu, Imaging Research for Neurodevelopment Laboratory, University of California San Francisco, 1700 4th Street, BH303B, UCSF Box 2532, San Francisco, CA 94158, USA.

Email: duan.xu@ucsf.edu

Funding information

The authors thank the funding support by the NIH R35 (5R35NS097299) (Donna M. Ferriero, Duan Xu), Academy of Finland (decision Nos. 326494, 326495, and 345280), and Research Council of Finland (decision No. 355256) (Tiina Manninen).

Abstract

Hypoxic-ischemic encephalopathy (HIE) is a common neurological syndrome in newborns with high mortality and morbidity. Therapeutic hypothermia (TH), which is standard of care for HIE, mitigates brain injury by suppressing anaerobic metabolism. However, more than 40% of HIE neonates have a poor outcome, even after TH. This study aims to provide metabolic biomarkers for predicting the outcomes of hypoxia-ischemia (HI) after TH using hyperpolarized [1-¹³C] pyruvate magnetic resonance spectroscopy. Postnatal day 10 (P10) mice with HI underwent TH at 1 h and were scanned at 6–8 h (P10), 24 h (P11), 7 days (P17), and 21 days (P31) post-HI on a 14.1-T NMR spectrometer. The metabolic images were collected, and the conversion rate from pyruvate to lactate and the ratio of lactate to pyruvate in the injured left hemisphere ($k_{PL(L)}$ and Lac/Pyr_(L), respectively) were calculated at each timepoint. The outcomes of TH were determined by the assessments of brain injury on T2-weighted images and behavioral tests at later timepoint. $k_{PL(L)}$ and Lac/Pyr_(L) over time between the good-outcome and poor-outcome groups and across timepoints within groups were analyzed. We found significant differences in temporal trends of $k_{PL(L)}$ and Lac/Pyr_(L) between groups. In the good-outcome group, $k_{PL(L)}$ increased until P31 with a significantly higher value at P31 compared with that at P10, while the level of Lac/Pyr_(L) at P31 was notably higher than those at all other timepoints. In the poor-outcome group, $k_{PL(L)}$ and Lac/Pyr_(L) increased within 24 h. The $k_{PL(L)}$ value at P11 was considerably higher compared with P10. Discrete temporal changes of $k_{PL(L)}$ and Lac/Pyr_(L) after TH between the good-outcome and poor-outcome groups were seen as early as 24 h after HI, reflecting various TH effects on brain anaerobic metabolism, which may provide insights for early screening for response to TH.

Abbreviations: bpm, breaths per minute; Cho, choline; Cr, creatine; CSI, chemical-shift imaging; DNP, dynamic nuclear polarization; EPP, exchangeable phosphate pool; FID, free induction decay; FOV, field of view; FSE, fast spin echo; GABA, gamma-aminobutyric acid; HI, hypoxia-ischemia; HIE, hypoxic-ischemic encephalopathy; HP, hyperpolarized; k_{PL} , conversion rate from pyruvate to lactate; Lac, lactate; Lac/Pyr, ratio of lactate to pyruvate; MD, mean diffusivity; NAA, N-acetylaspartate; NOR, novel object recognition; NTP, nucleotide triphosphate; PCr, phosphocreatine; Pi, inorganic phosphate; PI, preference index; RCT, randomized controlled trial; SNR, signal-to-noise ratio; T2WI, T2-weighted imaging; TCA, tricarboxylic acid; TE, echo time; TF, exploration time for the familiar object; TH, therapeutic hypothermia; TN, exploration time for the new object; TR, repetition time.

This is an open access article under the terms of the [Creative Commons Attribution-NonCommercial](https://creativecommons.org/licenses/by-nc/4.0/) License, which permits use, distribution and reproduction in any medium, provided the original work is properly cited and is not used for commercial purposes.

© 2024 The Author(s). *NMR in Biomedicine* published by John Wiley & Sons Ltd.

KEYWORDS

anaerobic metabolism, hyperpolarized [$1\text{-}^{13}\text{C}$] pyruvate MR spectroscopy, hypoxic-ischemic encephalopathy, therapeutic hypothermia

1 | INTRODUCTION

Neonatal hypoxic-ischemic encephalopathy (HIE), characterized by inadequate blood flow (ischemia) and oxygen (hypoxia) to the brain and other organs, affects 1.5–2 per 1000 live births in developed countries.¹ HIE to the developing brain contributes significantly to mortality and long-term morbidity, with at least 25% of surviving children exhibiting long-term neurodevelopmental sequelae ranging from mild to severe, including developmental delay intellectual disability, cerebral palsy, and epilepsy.² Previous studies have described the evolution of brain injury secondary to hypoxia-ischemia (HI) in four phases: (i) the acute phase, also known as “primary energy failure”, occurring within the first 6 h after injury and characterized by anaerobic metabolism, oxidative stress, neuronal cell death, and excitotoxicity; (ii) the latent phase, characterized by neuroinflammation and the continuation of activated apoptotic cascades occurring within 6–48 h; (iii) the secondary phase, also known as “secondary energy failure”, occurring within 48 h–7 days and characterized by cytotoxic edema, excitotoxicity, and cerebral hyperperfusion; and (iv) the tertiary phase, occurring in the weeks or months following primary energy failure, involving remodeling of injured brain, astrogliosis, and late cell death.^{3–5}

Therapeutic hypothermia (TH) is currently the standard of care for moderate to severe neonatal HIE. TH can ameliorate or lessen further brain injury during secondary energy failure if applied within 6 h after birth and continued for 72 h.¹ However, in multiple randomized controlled trials (RCTs) and in clinical practice, a significant number of neonates (40%–50%) suffered the composite outcome of death or disability despite receiving TH.⁶ At present, it is unclear why some infants have a good response to TH while others do not.

NMR spectroscopy is a useful technique that measures temporal changes in cellular metabolite levels and offers a snapshot of cerebral metabolic status *in vivo*.⁷ A few studies have utilized ^1H or ^{31}P magnetic resonance spectroscopy (MRS) to evaluate the status of brain metabolites and neurotransmitters in neonatal HI and the effects of TH on brain injury. ^1H MRS studies showed early elevations of lactate (Lac)/creatinine (Cr) and Lac/N-acetylaspartate (NAA) at 24 h after the insult which continued to worsen for 5–7 days in HI animal models and HIE neonates.^{8,9} The deep gray matter Lac/NAA is regarded as the strongest predictor for neurodevelopmental outcome after HIE, regardless of whether they received TH.¹⁰ The neuroprotective role of TH on brain injury results from changes in glucose metabolism (glucose and lactate concentration reduced) and neurotransmitters (glutamate, aspartate, and gamma-aminobutyric acid [GABA]) in neonates with HIE.¹¹ A previous animal ^{31}P MRS study demonstrated that the phosphocreatine (PCr)/inorganic phosphate (Pi) and nucleotide triphosphate (NTP)/exchangeable phosphate pool (EPP) were significantly higher in the hypothermic group compared with the normothermic group between 24 and 48 h after the HI insult and no further fall existed in either PCr/Pi or NTP/EPP up to 64 h in the hypothermic group, suggesting that TH after HI ameliorated secondary energy failure.¹²

Hyperpolarized ^{13}C MRS (HP ^{13}C MRS) is a new method enabling an entirely different avenue to study metabolism in real time. Dynamic nuclear polarization (DNP) is based on polarizing the nuclear spins of a molecule in the solid state, which is able to increase the ^{13}C NMR signal more than 10,000-fold, allowing investigation of the glucose metabolic pathway *in vivo*.¹³ Once HP [$1\text{-}^{13}\text{C}$] pyruvate is injected into a living animal, a real-time metabolic image can be performed to visualize the process of the pyruvate to lactate conversion within a short period of time.¹³ The measurements of the conversion rate from pyruvate to lactate (k_{PL}) and the ratio of lactate to pyruvate (Lac/Pyr) demonstrate the anaerobic metabolic rate (metabolic status) and the lactate levels in brain tissue. Our previous studies have described the anaerobic metabolic profile via the measurements of k_{PL} and lactate levels during brain development in normal and HI mouse using HP [$1\text{-}^{13}\text{C}$] pyruvate MRS.^{13,14} Additionally, TH preserves glucose reserves in the brain and lowers lactate levels, which has been proposed to be implicated in the beneficial effect of TH on the brain.¹⁵ In this study, we investigated the temporal changes of k_{PL} and Lac/Pyr following TH in HI mice using HP [$1\text{-}^{13}\text{C}$] pyruvate MRS, aiming to provide metabolic biomarkers for predicting the outcomes of HI after TH.

2 | MATERIALS AND METHODS

2.1 | HI model establishment and therapeutic hypothermia intervention

A total of 35 male and female CD-1 mice were subjected to HI, as previously described according to the Vannucci model,¹⁶ at postnatal day 10 (P10). Mice were anesthetized with 2%–2.5% isoflurane. A midline neck incision was performed to separate and permanently ligate the left common carotid artery via electrical coagulation. After the procedure, mice were allowed 1-h recovery with the dam. Global hypoxia was induced by placing the pups in chambers submerged in a water bath at 36.5°C, into which a hypoxia atmosphere of 10% O_2 /90% N_2 was

introduced via inlet and outlet tubing controlled by a flow meter for 1 h and then the pups were returned to the dam for 1 h. Subsequently, TH was performed by placing the mice in chambers submerged in a water bath at 30°C for 3.5 h.^{17–19} The body temperature range of mice was 29.0–30.5°C during this procedure. After TH, the mice were allowed to rewarm for 15 min before being returned to the nest. The body temperature range of mice recovered to 35.5–36.5°C. All procedures and MR scans were approved by the Institutional Animal Care and Use Committee at the University of California San Francisco, in accordance with the National Institutes of Health guidelines for the Care and Use of Laboratory Animals.

2.2 | MRS acquisition

Mice were scanned at 6–8 h (P10) or 24 h (P11), 7–12 days (P17–P22) and 21–29 days (P31–P39) post-HI. These timepoints were chosen to span murine brain maturation, with P10 and P11 being equivalent to human infants at term, P17 being representative of early childhood, and P31 being representative of adolescence.²⁰ Forty-eight microliters of C-1 labeled ¹³C pyruvic acid was polarized in an Oxford Hypersense DNP instrument at 3.5 T under 1.4 K for ~1 h. Before injection, the HP C-1 labeled ¹³C pyruvate was mixed with 4.5 mL of NaOH buffer, resulting in a 160 mM pyruvate solution with ~pH 7. Mice were anesthetized with 2%–2.5% isoflurane and tail vein cannulation was performed before scans.

Mice were anesthetized with 1%–1.5% isoflurane and 1 L/min oxygen during scans. Vital signs were carefully monitored, maintaining the respiratory rate around 30 breaths per minute (bpm) and the body temperature was maintained within a range of 36.5–37°C. A total volume of 250–300 µL pyruvate solution (150 µL dead volume in the catheter) was then delivered through the tail vein catheter over a span of 12 s during MR scans. The smaller volume was used for P10 or P11 mice to ensure a better survival rate after injection. Thirty microliters of mixed saline and heparin solution was injected into the catheter every 15 min to prevent blood clots.

MR scans were conducted on a vertical 14.1-T (Varian/Agilent) 600 WB NMR spectrometer with 55-mm 1000 mT/m gradients. A 38-mm diameter ¹H and ¹³C dual-tuned coil was used for main field shimming and T2-weighted anatomical imaging (¹H frequency) and for HP ¹³C spectroscopic imaging (¹³C frequency). The ¹³C spectroscopic imaging data were acquired on a 24 mm × 24 mm × 5 mm slice centered on the brain, with 2D chemical-shift imaging (CSI). Center-out k-space trajectory²¹ was used with 7 × 7 phase encoding (zero-filled to 8 × 8). One hundred and twenty-eight spectral points were acquired with 2500-Hz bandwidth. The acquisition was initiated immediately after the pyruvate injection to capture the entire course of pyruvate conversion. The acquisition was repeated every 4 s (3-s acquisition time with 1-s delay between each repetition) for a total of 60 s (15 repetitions) with a contrast flip angle of 10°. The 2D fast spin echo (FSE) sequence was applied for the T2-weighted anatomical imaging with repetition time (TR)/echo time (TE) = 1300 ms/12 ms, and eight echo train lengths with 12-ms echo spacing. The field of view (FOV) was 30 mm × 30 mm with 256 frequency and phase encodes, resulting in a 0.12 mm × 0.12 mm in-plane resolution. The slice thickness was 1 mm, and 10 slices were acquired without gap, covering most of the brain. The total scan time was 11 min.

2.3 | Evaluation of brain damage

The T2 score was regarded as a reliable metric for assessing the extent of brain injury in HI mice on T2-weighted imaging (T2WI).^{22,23} The evaluation of T2 score was based on the three major areas affected (i.e., the cortex, hippocampus, and deep gray nuclei) and the intensity of the lesions on T2WI. Each area was scored from rostral to caudal by progressively increasing numerical scores.¹³ More specifically, each area was scored from 0 to 3 based on the following standard: 0 for no injury observed, 1 for a mild focal hyperintensity, 2 for a large hyperintensity that expanded to adjacent areas, and 3 for a cystic infarction. The total score was the sum of the three areas and ranged from 0 to 9. All mice had T2 scores measured after the MR scan at each timepoint.

2.4 | Data processing and analysis

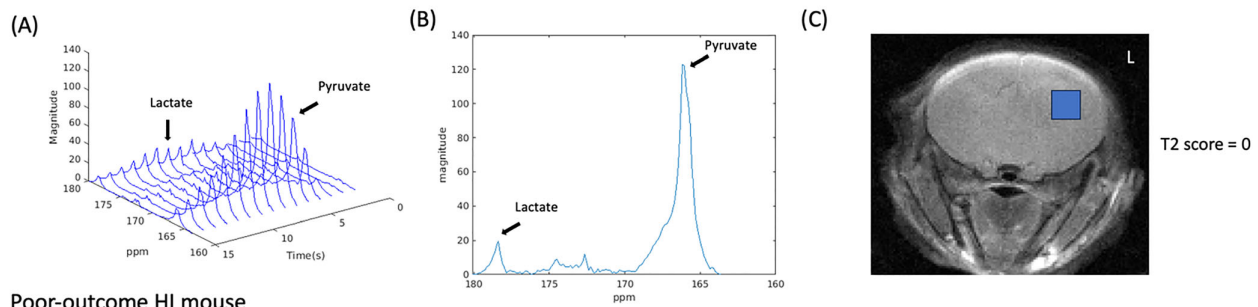
Each dynamic raw free induction decay (FID) of the 2D CSI acquisitions was apodized with 10-Hz Lorentzian filter, then zero-filled to double the resolution in both spatial dimensions, before Fourier reconstruction using SIVIC software (<https://sourceforge.net/projects/sivic/>). Once the 5D data were read into MATLAB software (version 2019a; <https://www.mathworks.com/products/matlab.html>), the tensor denoising and the phase and baseline corrections were performed. The dynamic area under the curve (AUC) maps for pyruvate and lactate were obtained by taking the sum of magnitude values in the peak ranges for both lactate and pyruvate. Simultaneously, the peak height maps were obtained by taking the maximum magnitude values in the peak ranges. The k_{PL} map was generated by fitting the dynamic AUC maps and the dynamic peak height maps on a voxel-wise basis for each dynamic voxel (<https://github.com/LarsonLab/hyperpolarized-mri-toolbox>). Parameters for fitting

corresponded to the acquisition parameters and known relaxation times. Only voxels inside of segmented mouse brain regions of interest were used in downstream analysis, to prevent inclusion of k_{PL} values from the noisy spectra and the areas of poor signal-to-noise ratio (SNR).²⁴ Subsequently, the mean k_{PL} value, as well as the total sum of the AUCs of lactate and pyruvate through time for the corresponding left and right sides of the brain, were calculated. The Lac/Pyr value was calculated by the ratio of the summed AUCs of the lactate to the summed AUCs of the pyruvate for the left and right hemisphere through time. Figure 1 shows the HP ^{13}C spectra of two P11 HI mice from the good-outcome group and the poor-outcome group, respectively.

2.5 | Behavioral tests

The novel object recognition (NOR) test and cylinder test were regarded as the optimal behavioral tests for evaluating the cognitive function (learning and memory) and motor control in HI mice.²⁵ All mice performed behavioral tests at P31–39 after the MR scans. In the NOR test, mice were tested for 4 consecutive days: habituation day, training day, and testing day. On habituation day (days 1 and 2), all the mice of a single cage were placed in the testing box (40 cm × 40 cm × 30 cm) for 10 min, then each mouse was placed alone in the testing box for 5 min. On training day (day 3), the mice were allowed to freely explore two identical objects in the testing box for 5 min. On testing day (day 4), one of the training objects was replaced with a novel object, and the mice were allowed to freely explore objects in the testing box for 3 min. The object exploration was defined when the mouse was in proximity (< 1 cm) to the objects. The exploration time for the familiar object (TF) and the exploration time for the new object (TN) were recorded. The NOR percentage (NOR %) was calculated as: $\text{TN} / (\text{TN} + \text{TF}) \times 100$.²⁶ In the cylinder test, mice with unilateral brain injury exhibited forelimb preference shown by favoring use of the nonimpaired limb (ipsilateral) for touching or bracing the side of the cylinder. During the test, mice were placed in a transparent plexiglass container (20-cm diameter, 30-cm height) and the initial forepaw placement was recorded as left (ipsilateral), right (contralateral), or both. Two trials were conducted on consecutive days and each trial lasted 3 min. The preference index (PI %) was calculated as: $(\text{left} - \text{right}) / (\text{left} + \text{right} + \text{both}) \times 100$.²⁷

Good-outcome HI mouse



Poor-outcome HI mouse

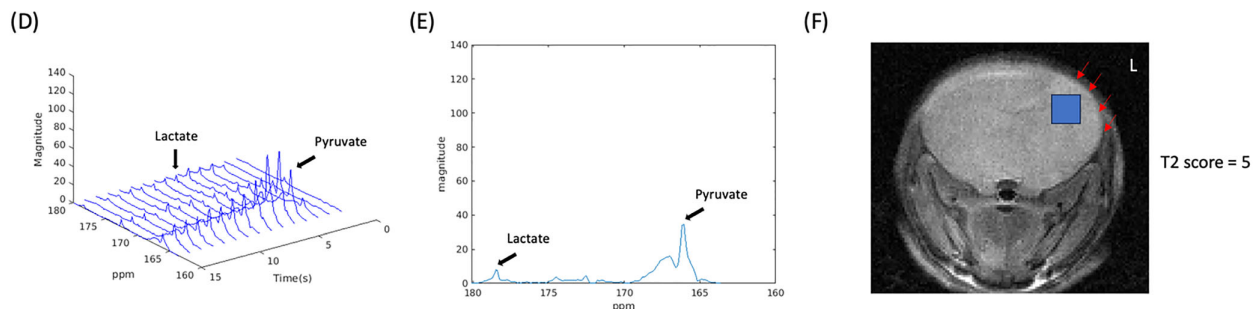


FIGURE 1 The hyperpolarized ^{13}C spectra of two P11 hypoxia-ischemia (HI) mice from the good-outcome group and the poor-outcome group, respectively. (A) A stack plot of sequential spectra of the selected voxel (blue square in (C)) during the 15 s in a HI mouse from the good-outcome group. (B) A single spectrum of the selected voxel (blue square in (C)) at 8 s in a HI mouse from the good-outcome group. (C) T2-weighted magnetic resonance (MR) image of a HI mouse from the good-outcome group. There is no visible brain injury (the T2 score is 0). The selected voxel (blue square) for drawing the spectra was in the region that covers the left deep gray nucleus (putamen) and cortex. (D) A stack plot of sequential spectra of the selected voxel (blue square in (F)) during the 15 s in a HI mouse from the poor-outcome group. (E) A single spectrum of the selected voxel (blue square in (F)) at 8 s in a HI mouse from the poor-outcome group. (F) T2-weighted MR image of a HI mouse from the poor-outcome group. There is a brain injury with mild hyperintensity (the T2 score is 5; red arrows). The selected voxel (blue square) for drawing the spectra was placed in the brain injury region that covers the left deep gray nucleus (putamen) and cortex.

2.6 | Statistical analysis

2.6.1 | Group classification based on outcomes following TH

The outcomes of TH were determined by the T2 score at P17–P22 and the assessments of behavioral tests (NOR test and cylinder test) at P31–P39. For some mice that were missing scans or had poor image quality at P17–P22, we used the T2 score at P31–P39, which had an injury pattern similar to the injury at P17–P22. The T2 score and the assessments of the NOR test (NOR %) and cylinder test (PI %) of all mice were standardized and then were used to classify all mice into the good-outcome group and the poor-outcome group by the k-means clustering method using R studio (AGPL v3; <https://support-rstudio-com.netlify.app/products/rstudio/#rstudio-server>). The Mann–Whitney test was used to compare the T2 scores and behavioral measurements between the good-outcome group and the poor-outcome group using SPSS v. 27 software. The statistical significance was set at p less than 0.05.

2.6.2 | Comparisons in the temporal changes of the metabolic metrics in the injured left hemisphere between groups

The mixed model for repeated measures (MMRM) was used to compare the temporal changes of k_{pL} and Lac/Pyr in the injured left hemisphere ($k_{pL(L)}$ and Lac/Pyr_(L)) between the good-outcome group and the poor-outcome group using SPSS v. 27 software. Post-hoc tests were further used to investigate the main effects on the group and timepoints. Bonferroni correction was used for multiple comparisons. The statistical significance was set at p less than 0.05.

2.6.3 | Comparisons of the metabolic metrics in the injured left hemisphere across different timepoints within each group

A Kruskal–Wallis one-way analysis of variance (ANOVA) was used to investigate the $k_{pL(L)}$ and Lac/Pyr_(L) values across different timepoints in the good-outcome group and the poor-outcome group. Post-hoc tests with Bonferroni correction were used for multiple comparisons. All statistical analyses were performed using SPSS v. 27 software. The statistical significance was set at p less than 0.05.

2.6.4 | Comparisons of the metabolic metrics in the injured left hemisphere between groups at each timepoint

The Mann–Whitney test was used to compare the $k_{pL(L)}$ and Lac/Pyr_(L) values between the good-outcome group and the poor-outcome group at each timepoint. All statistical analyses were performed using SPSS v. 27 software. The statistical significance was set at p less than 0.05.

3 | RESULTS

3.1 | Group classification of the response to TH

Two of 35 mice died during the experimental procedure, setting the mortality rate at 5.7%. Four of 35 mice were excluded because of poor ¹³C MR spectra or missing MR data due to acquisition failure. A total of 29 mice were included in the study. The cluster plots (Figure 2A,B) show the results of the k-means clustering analysis. We observed that the T2 scores of the mice in cluster 1 were less than 5, and that these mice had a better performance in the behavioral tests. Thus, we defined cluster 1 as the good-outcome group, and cluster 2 as the poor-outcome group. Some mice who did not complete the behavioral tests ($n = 8$) were classified based on the T2 score at P31–P39. The ones whose T2 score was less than 5 were included in the good-outcome group, while the others were assigned to the poor-outcome group. Fifteen of 29 mice were included in the good-outcome group and 14 of 29 mice were included in the poor-outcome group. Because of scanner availability and technical issues, some scan dates were slightly shifted or MR data at some timepoints were missing. Compared with the poor-outcome group, the good-outcome group showed significantly lower T2 scores and PI % ($p < 0.001$, two tailed) (Table 1 and Figure 2C,E). There was no significant difference in NOR % between the good-outcome group and the poor-outcome group (Figure 2D).

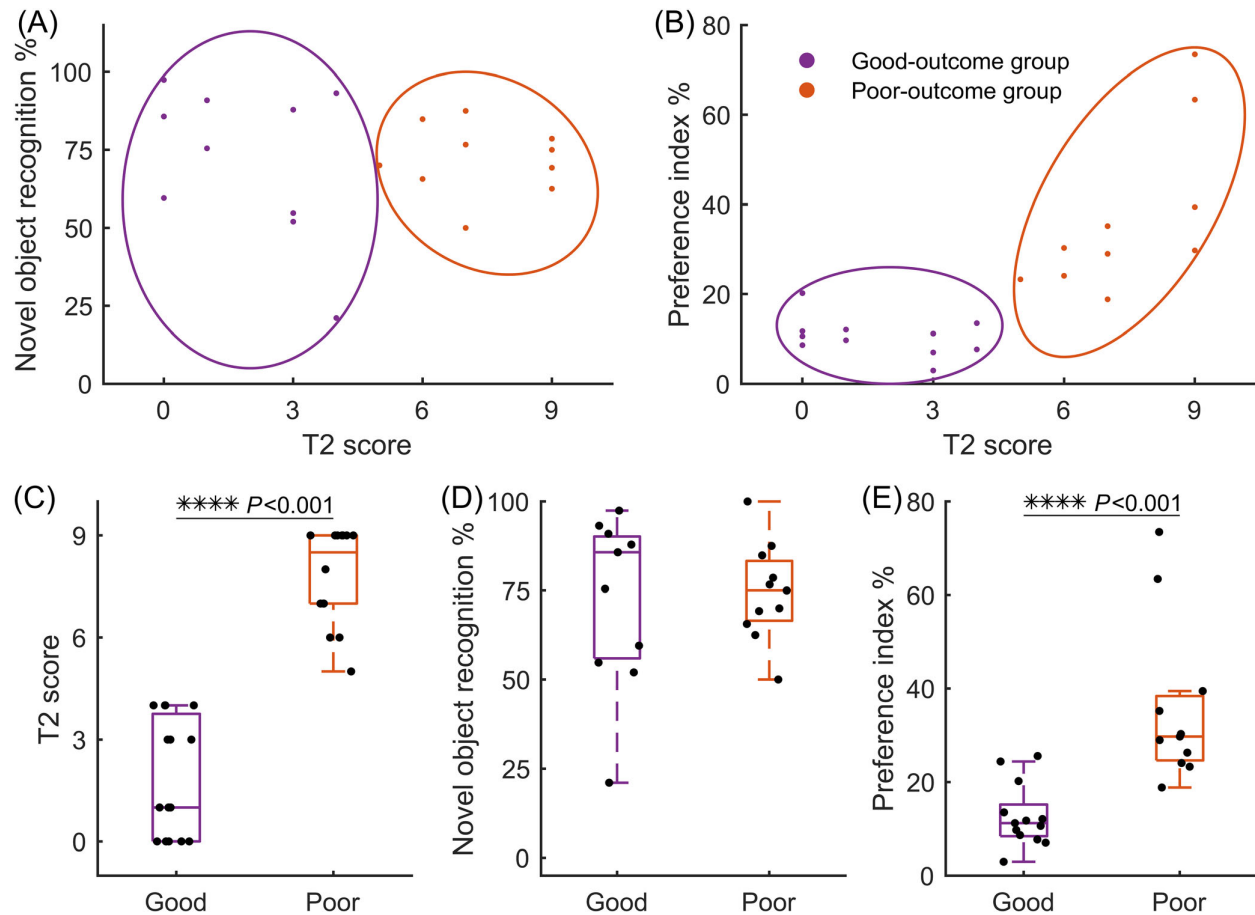


FIGURE 2 The T2 score and behavioral assessments of the good-outcome group and the poor-outcome group. (A) and (B) Cluster plots show the k-means clustering based on T2 score, novel object recognition percentage (NOR %), and preference index (PI %). (C)–(E) Boxplots with scatters show the differences in T2 scores, NOR % and PI % between the good-outcome group and the poor-outcome group. **** $p < 0.001$.

TABLE 1 Comparisons of T2 score and behavioral assessments between the good-outcome group and the poor-outcome group.

	Good-outcome group (mean \pm SD)	Poor-outcome group (mean \pm SD)	<i>p</i> value
T2 score (good-outcome group: $n = 15$, poor-outcome group: $n = 14$)	1.9 ± 1.7	7.8 ± 1.4	< 0.001 ****
Novel object exploration ratio (%) (good-outcome group: $n = 11$, poor-outcome group: $n = 11$)	73.1 ± 23.5	74.5 ± 13.5	0.70
Preference index (%) (good-outcome group: $n = 13$, poor-outcome group: $n = 11$)	12.7 ± 6.7	35.7 ± 17.3	< 0.001 ****

Abbreviation: SD, standard deviation.

**** $p < 0.001$.

3.2 | Significant differences in the temporal changes of the conversion rate of pyruvate to lactate in the injured left hemisphere between groups

Figure 3A,B show the individual temporal change of $k_{PL(L)}$ in the good-outcome group and the poor-outcome group, respectively. After MMRM analysis, we found a significant difference in the temporal change of $k_{PL(L)}$ between the good-outcome group and the poor-outcome group ($p_{\text{group} \times \text{time}} < 0.05$, two-tailed). In addition, we detected significant differences in $k_{PL(L)}$ across different timepoints ($p_{\text{time}} < 0.01$, two-tailed) (Figure 3C). Specifically, the $k_{PL(L)}$ value was significantly higher at P31–P39 compared with P10 ($p < 0.005$, two-tailed). To further understand the temporal changes of $k_{PL(L)}$ within each group, we performed a Kruskal–Wallis one-way ANOVA. We found that the $k_{PL(L)}$ increased from P10

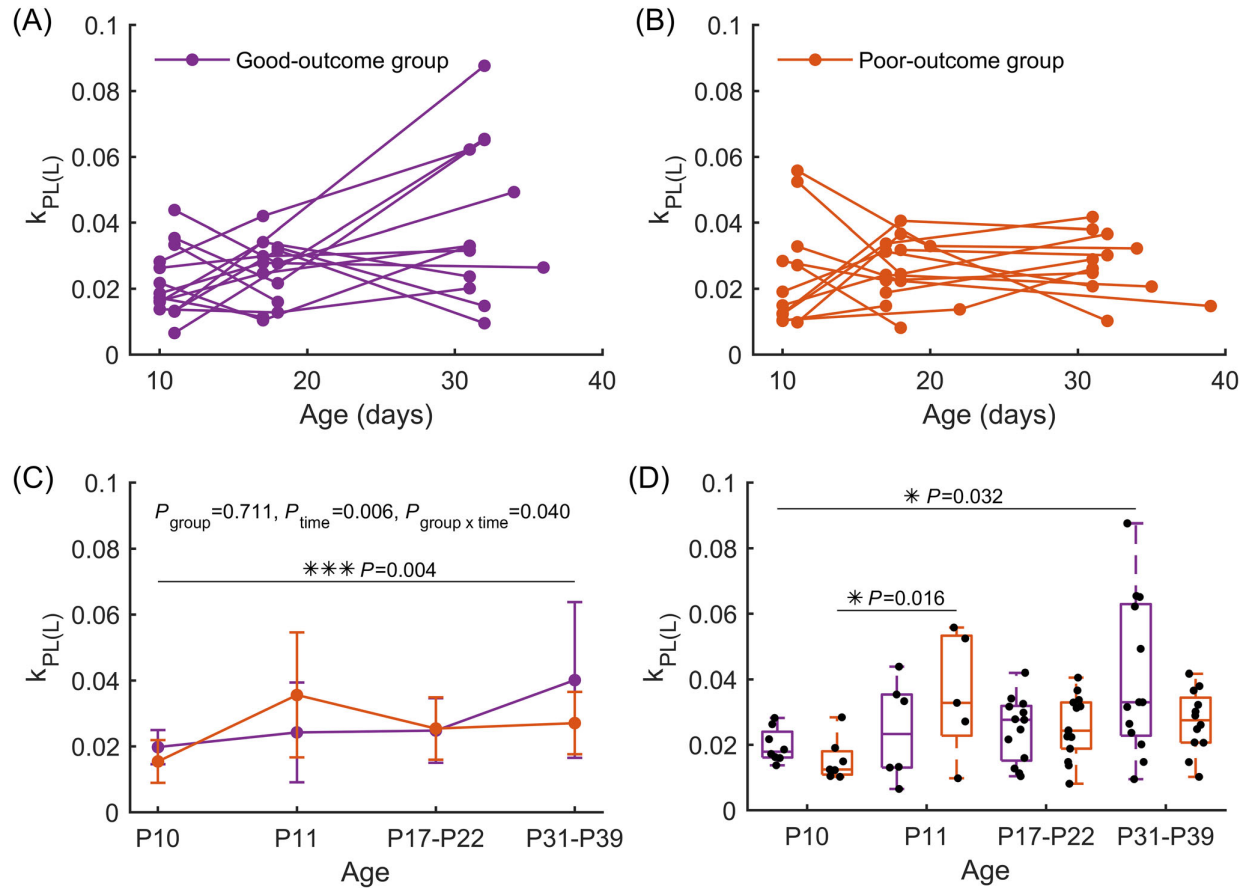


FIGURE 3 The temporal changes of conversion rate from pyruvate to lactate in the injured left hemisphere ($k_{PL(L)}$) between the good-outcome group and the poor-outcome group. (A) The line graph shows the individual temporal change of $k_{PL(L)}$ in the good-outcome group. (B) The line graph shows the individual temporal change of $k_{PL(L)}$ in the poor-outcome group. (C) The line graph shows the temporal changes in the mean value and standard deviation of $k_{PL(L)}$ in the good-outcome group (purple line) and the poor-outcome group (orange line). There was a significant difference in the temporal trend of $k_{PL(L)}$ between the good-outcome group and the poor-outcome group ($p_{\text{group} \times \text{time}} < 0.05$, two-tailed) and a significant difference in the $k_{PL(L)}$ value across different timepoints ($p_{\text{time}} < 0.01$, two-tailed). Specifically, the $k_{PL(L)}$ value was significantly higher at P31–P39 compared with at P10 ($p < 0.005$, two-tailed). (D) The boxplot shows the 25th percentile, the 50th percentile (median), and the 75th percentile values of $k_{PL(L)}$ in the good-outcome group (purple box) and the poor-outcome group (orange box) at each timepoint. The $k_{PL(L)}$ value at P31–P39 was significantly higher compared with P10 in the good-outcome group ($p < 0.05$, two-tailed), while the $k_{PL(L)}$ value at P11 was significantly higher compared with P10 in the poor-outcome group ($p < 0.05$, two-tailed). * $p < 0.05$, *** $p < 0.005$.

to P31–P39 and that the $k_{PL(L)}$ value was significantly higher at P31–P39 compared with P10 in the good-outcome group ($p < 0.05$, two-tailed), while $k_{PL(L)}$ increased from P10 to P11, decreased at P17–P22, and then slowly increased until P31–P39 in the poor-outcome group. The $k_{PL(L)}$ at P11 was significantly higher compared with P10 ($p < 0.05$, two-tailed) (Figure 3D and Table 2).

3.3 | Significant differences in the temporal changes in the ratio of pyruvate to lactate in the injured left hemisphere between groups

Figure 4A,B show the individual temporal change of Lac/Pyruvate in the good-outcome group and the poor-outcome group, respectively. After MMRM analysis, we found a significant difference in the temporal change of Lac/Pyruvate between the good-outcome group and the poor-outcome group ($p_{\text{group} \times \text{time}} < 0.05$, two-tailed). In addition, we detected significant differences in Lac/Pyruvate across different timepoints ($p_{\text{time}} < 0.001$, two-tailed) (Figure 4C). Specifically, the Lac/Pyruvate value was significantly higher at P31–P39 compared with other timepoints (P10 vs. P31–P39: $p < 0.001$ [two-tailed], P11 vs. P31–P39: $p < 0.05$ [two-tailed], P17–P22 vs. P31–P39: $p < 0.001$ [two-tailed]). To further understand the temporal changes of Lac/Pyruvate within each group, we performed a Kruskal–Wallis one-way ANOVA. We found that Lac/Pyruvate decreased at P11 and then

TABLE 2 Comparisons of metabolic metrics in the injured left hemisphere between the good-outcome group and the poor-outcome group.

	P10 (6–8 h post-HI) (good-outcome group: <i>n</i> = 8, poor-outcome group: <i>n</i> = 7)	P11 (24-h post-HI) (good-outcome group: <i>n</i> = 6, poor-outcome group: <i>n</i> = 5)	P17–P22 (7–12 days post-HI) (good-outcome group: <i>n</i> = 13, poor- outcome group: <i>n</i> = 14)	P31–P39 (21–29 days post-HI) (good-outcome group: <i>n</i> = 13, poor- outcome group: <i>n</i> = 12)	<i>p</i> value
Good-outcome group					
$k_{PL(L)}$ (mean \pm SD)	0.02 \pm 0.01	0.02 \pm 0.02	0.02 \pm 0.01	0.04 \pm 0.02	P10 vs. P31 <i>p</i> = 0.032*
Lac/Py _{r(L)} (mean \pm SD)	0.19 \pm 0.05	0.17 \pm 0.09	0.21 \pm 0.08	0.38 \pm 0.15	P10 vs. P31 <i>p</i> = 0.007** P11 vs. P31 <i>p</i> = 0.006** P17 vs. P31 <i>p</i> = 0.008**
Poor-outcome group					
$k_{PL(L)}$ (mean \pm SD)	0.02 \pm 0.01	0.04 \pm 0.02	0.03 \pm 0.01	0.03 \pm 0.01	P10 vs. P11 <i>p</i> = 0.016*
Lac/Py _{r(L)} (mean \pm SD)	0.18 \pm 0.08	0.25 \pm 0.10	0.21 \pm 0.06	0.27 \pm 0.10	

Abbreviations: HI, hypoxia-ischemia; $k_{PL(L)}$, conversion rate from pyruvate to lactate in the injured left hemisphere; Lac/Py_{r(L)}, ratio of lactate to pyruvate in the injured left hemisphere; P10, postnatal day 10; P11, postnatal day 11; P17, postnatal day 17; P22, postnatal day 22; P31, postnatal day 31; P39, postnatal day 39; SD, standard deviation.

p* < 0.05. *p* < 0.01.

increased until P31–P39, with a significantly higher Lac/Py_{r(L)} value at P31–P39 compared with other timepoints in the good-outcome group (P10 vs. P31–P39: *p* < 0.01 [two-tailed], P11 vs. P31–P39: *p* < 0.01 [two-tailed], P17–P22 vs. P31–P39: *p* < 0.01 [two-tailed]), while Lac/Py_{r(L)} increased from P10 to P11, decreased from P11 to P17–P22, and then increased until P31–P39 in the poor-outcome group, but there were no significant differences in the Lac/Py_{r(L)} value across all timepoints (Figure 4D and Table 2).

3.4 | No significant differences in the conversion rate of pyruvate to lactate and the ratio of pyruvate to lactate in the injured left hemisphere between groups at each timepoint

After Mann–Whitney analysis, we did not detect significant differences in the $k_{PL(L)}$ and Lac/Py_{r(L)} values between the good-outcome group and the poor-outcome group at P10, P11, P17–P22, and P31–P39 (Figures 3D, 4D, and Table 2).

4 | DISCUSSION

This is the first study to evaluate the effects of TH on cerebral glucose metabolism after HI during brain development in murine using HP [1-¹³C] pyruvate MRS. In this study, we identified the good-outcome group and the poor-outcome group based on the T2 scores at P17–P22 and the assessments of behavioral tests (NOR and cylinder tests) at P31–P39 using k-means clustering methods. Compared with the poor-outcome group, the good-outcome group had significantly lower T2 scores and lower PI. Intriguingly, we found discrete temporal changes of k_{PL} and Lac/Py_r in the injured left hemisphere between these two groups. In the good-outcome group, an increased trend of $k_{PL(L)}$ was seen from P10 to P31–P39 and the $k_{PL(L)}$ value at P31–P39 was significantly higher compared with at P10, while Lac/Py_{r(L)} decreased within 24 h and then increased until P31–P39, with a significantly higher Lac/Py_{r(L)} value at P31–P39 compared with other timepoints. In the poor-outcome group, $k_{PL(L)}$ and Lac/Py_{r(L)} increased within 24 h, decreased at P17–P22, and then slowly increased until P31–P39. The $k_{PL(L)}$ value at P11 was significantly higher compared with P10, but no significant differences in the Lac/Py_{r(L)} values were seen across all timepoints.

Glucose plays a critical role in maintaining cerebral energy demands in the immature brain, although the immature brain utilizes other substrates as well, such as the ketone bodies and lactate, in the presence of oxygen.²⁸ During HI, glucose is the only substrate capable of sustaining cerebral energy demands.²⁹ Glucose is metabolized into pyruvate, which can then either be converted anaerobically to lactate or alanine or enter the tricarboxylic acid (TCA) cycle to produce adenosine triphosphate (ATP).²⁹ However, the insufficient delivery of glucose due to hypoperfusion leads to energy failure and cell death. In addition, hypoperfusion influences the clearance of lactic acid, resulting in lactate accumulation and cellular acidosis. Conducting TH within 6 h after HI has been demonstrated to preserve the glucose reserve and has neuroprotective effects on brain

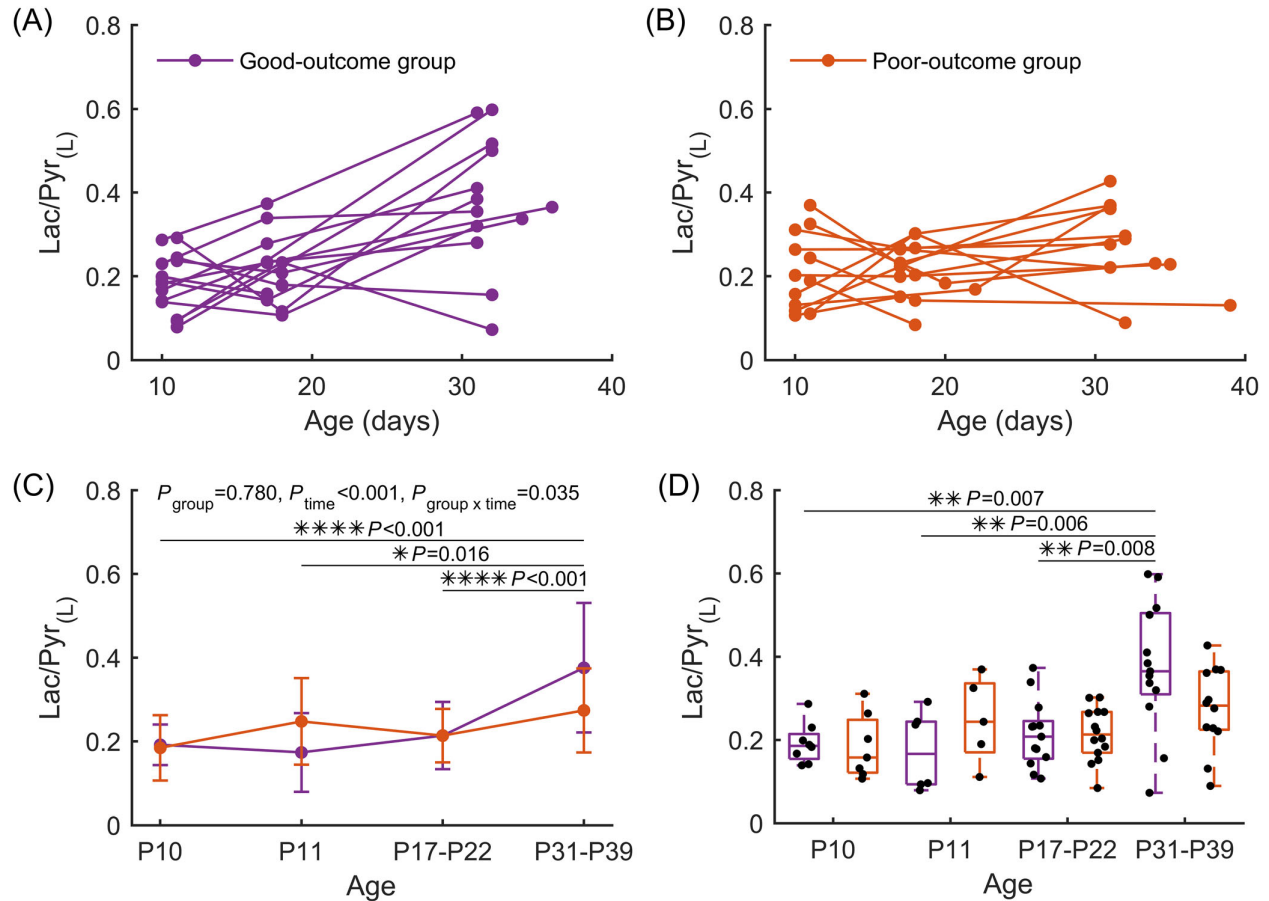


FIGURE 4 The temporal changes of the ratio of lactate to pyruvate in the injured left hemisphere ($Lac/Pyruv_{(L)}$) between the good-outcome group and the poor-outcome group. (A) The line graph shows the individual temporal change of $Lac/Pyruv_{(L)}$ in the good-outcome group. (B) The line graph shows the individual temporal change of $Lac/Pyruv_{(L)}$ in the poor-outcome group. (C) The line graph shows the temporal changes in the mean value and standard deviation of $Lac/Pyruv_{(L)}$ in the good-outcome group (purple line) and the poor-outcome group (orange line). There was a significant difference in the temporal trend of $Lac/Pyruv_{(L)}$ between the good-outcome group and the poor-outcome group ($p_{group \times time} < 0.05$, two-tailed) and a significant difference in $Lac/Pyruv_{(L)}$ value across different timepoints ($p_{time} < 0.001$, two-tailed). Specifically, the $Lac/Pyruv_{(L)}$ value was significantly higher at P31–P39 compared with at other timepoints (P10 vs. P31–P39: $p < 0.001$ [two-tailed], P11 vs. P31–P39: $p < 0.05$ [two-tailed], P17–P22 vs. P31–P39: $p < 0.001$ [two-tailed]). (D) The boxplot shows the 25th percentile, the 50th percentile (median), and the 75th percentile values of $Lac/Pyruv_{(L)}$ in the good-outcome group (purple box) and the poor-outcome group (orange box) at each timepoint. The $Lac/Pyruv_{(L)}$ value at P31–P39 was significantly higher compared with those at other timepoints in the good-outcome group (P10 vs. P31–P39: $p < 0.01$ [two-tailed], P11 vs. P31–P39: $p < 0.01$ [two-tailed], P17–P22 vs. P31–P39: $p < 0.01$ [two-tailed]), while the $Lac/Pyruv_{(L)}$ value was not significantly different across timepoints in the poor-outcome group. * $p < 0.05$, ** $p < 0.01$, **** $p < 0.001$.

tissue in animal and human studies.^{30–33} In this study, TH was performed 1-h post-HI. Within the first 24 h after HI, we found an overt increase of $k_{PL(L)}$ at P11 compared with at P10 in the poor-outcome group, which indicates that mouse brain did not respond to TH and maintained higher rates of anaerobic metabolism, which converts pyruvate to lactate, in order to compensate for the energy failure. In contrast to the poor-outcome group, we did not see a significant difference in $k_{PL(L)}$ between P10 and P11 in the good-outcome group, which suggests that mouse brain had a good response to TH in suppressing the anaerobic metabolic rate. The different responses to TH between the good-outcome group and the poor-outcome group were also reflected by $Lac/Pyruv_{(L)}$. We found an increased trend of $Lac/Pyruv_{(L)}$ in the poor-outcome group, while there was a decreased trend of $Lac/Pyruv_{(L)}$ in the good-outcome group from P10 to P11. These findings are supported by a recent clinical study, which demonstrated an increase of plasma $Lac/Pyruv$ in the HIE neonates with pathological MRI and a decrease of plasma $Lac/Pyruv$ in the HIE neonates with normal MRI within 24 h after TH.³⁴ The decline of $Lac/Pyruv$ in the good-outcome group reflects the neuroprotective effects of TH by lowering the lactate accumulation to avoid lactic acidosis. Additionally, compared with the measurement of plasma $Lac/Pyruv$ that reflects the anaerobic metabolic status in all affected organs of the whole body, our HP [1-¹³C] pyruvate MRS technique provides more accurate information on the anaerobic metabolic status specifically in brain tissue, which has the potential to translate to the clinic.

During brain development, lactate can be used as an energy fuel to support neuronal and astrocytic function and synaptogenesis.^{35,36} It has been shown in rats that lactate utilization increased dramatically during the suckling period (P15–P21) and then decreased after weaning (P28).^{37,38} Our previous studies on the anaerobic metabolism during normal murine brain development demonstrated that the lactate levels significantly increased from P10 to P17 and then high levels were maintained after P17.^{13,14} In this study, we found an increased trend of $k_{PL(L)}$ and Lac/Pyr_(L) from P11 to P31–P39 and significantly higher values of $k_{PL(L)}$ and Lac/Pyr_(L) at P31–P39 in the good-outcome group, which indicates the neuroprotective contribution of TH in the early stage of HI, maintaining sufficient active brain tissue for anaerobic metabolism and lactate production during brain development. We also observed better behavioral performance in the good-outcome group at P31–P39, which provides evidence that TH helps to protect the brain tissue and is beneficial for brain development. In the poor-outcome group, we detected decreased $k_{PL(L)}$ and Lac/Pyr_(L) from P11 to P17–P22, which is similar to our previous observation of the alteration in lactate levels during the same age period in HI mice with visible brain injury (T2 score = 1–9).¹³ We interpreted this as a lack of active brain tissue capable of conducting anaerobic metabolism and lactate production for the energy demands during brain development, as documented in our previous study. In this study, we also noticed a significantly higher T2 score with cystic formation at P17–P22 in the poor-outcome group, indicating brain tissue loss. Therefore, the decline of $k_{PL(L)}$ and Lac/Pyr_(L) from P11 to P17–P22 might be attributable to a lack of response to TH in brain at the early stage after HI, which results in brain tissue loss and influences the anaerobic metabolism rate and lactate production. In addition, we found increased trends of $k_{PL(L)}$ and Lac/Pyr_(L) between P17–P22 and P31–P39 in the poor-outcome group, but the $k_{PL(L)}$ and Lac/Pyr_(L) values at P17–P22 did not significantly differ from those at P31–P39. This finding suggests that the remaining brain maintains the capacity of anaerobic metabolism, but the lactate level is below normal and might influence normal brain development, which is further reflected by the poor behavioral performance in the poor-outcome group.

In this study, we did not find significant differences in the $k_{PL(L)}$ and Lac/Pyr_(L) values at 6–8 h (P10), 24 h (P11), 7–12 days (P17–P22), and 21–29 days (P31–P39) post-HI between the good-outcome group and the poor-outcome group. A clinical study also demonstrated that the plasma Lac/Pyr was not significantly different between the normal and pathologic MRI outcomes in newborns who were diagnosed with HIE at 24 h after cooling,³⁴ suggesting that the measurement of Lac/Pyr might not be sensitive enough to discriminate between the good-outcome and the poor-outcome groups at early timepoints after TH. Another clinical study found a significant difference in the thalamic Lac/NAA at 4–16 days after HI between the HIE neonates with normal neurodevelopmental outcome and the HIE neonates with adverse neurodevelopmental outcome using ¹H-MRS.³⁹ However, in our mouse model, there were no differences in the $k_{PL(L)}$ and Lac/Pyr_(L) values at 7–12 days (P17–P22) post-HI between the good-outcome group and the poor-outcome group, but the group differences in the $k_{PL(L)}$ and Lac/Pyr_(L) values were enhanced at 21–29 days (P31–P39) post-HI. Whether the group differences in $k_{PL(L)}$ and Lac/Pyr_(L) values will reach significance after 30 days post-HI is a point for further study. Furthermore, other metabolic biomarkers, that is, NAA/Cr and NAA/Cho in the basal ganglia, were found to discriminate between the HIE neonates with normal and pathological/adverse neurodevelopmental outcomes and had positive predictive values for outcomes after TH in clinical studies.^{39,40} In the HP ¹³C field, [2-¹³C] pyruvate has been used to investigate aerobic (glutamate is a metabolic product of α -ketoglutarate in the TCA cycle) metabolism and anaerobic metabolism (pyruvate and lactate) at the same time in rodent and human studies.^{41,42} By leveraging HP [2-¹³C] pyruvate MRS to detect the dynamic changes of the metabolites from the aerobic and anaerobic metabolism after TH, we may recognize sensitive metabolic biomarkers for predicting outcomes after TH in the HI mouse model and in HIE neonates.

In conclusion, using HP [1-¹³C] pyruvate MRS, one can investigate the brain anaerobic metabolism following TH in HI mice in vivo. Although the metabolic measurements of $k_{PL(L)}$ and Lac/Pyr_(L) were not sensitive enough for discriminating the good-outcome group and the poor-outcome group, the discrete temporal changes of $k_{PL(L)}$ and Lac/Pyr_(L) between the good-outcome group and the poor-outcome group were seen as early as 24 h after HI insult, and therefore could enable early identification of infants at risk of further brain injury.

ACKNOWLEDGMENTS

The authors thank the funding support by the NIH R35 (5R35NS097299) (DF, DX) Academy of Finland (decision Nos. 326494, 326495, and 345280), Research Council of Finland (decision No. 355256) (TM), and NIH P41 5P41EB013598.

CONFLICT OF INTEREST STATEMENT

The authors declare no conflicts of interest.

DATA AVAILABILITY STATEMENT

The data that support the findings of this study are available from the corresponding author upon reasonable request.

ORCID

Xiaodan Liu  <https://orcid.org/0000-0003-1500-9086>

REFERENCES

1. Oorschot DE, Sizemore RJ, Amer AR. Treatment of neonatal hypoxic-ischemic encephalopathy with erythropoietin alone, and erythropoietin combined with hypothermia: History, current status, and future research. *Int J Mol Sci*. 2020;21(4):1487. doi:10.3390/ijms21041487
2. Vannucci RC. Current and potentially new management strategies for perinatal hypoxic-ischemic encephalopathy. *Pediatrics*. 1990;85:961-968. doi:10.1542/peds.85.6.961
3. Kleuskens DG, Gonçalves Costa F, Annink KV, et al. Pathophysiology of cerebral hyperperfusion in term neonates with hypoxic-ischemic encephalopathy: a systematic review for future research. *Front Pediatr*. 2021;9:631258. doi:10.3389/fped.2021.631258
4. Davidson JO, Gonzalez F, Gressens P, Gunn AJ, Newborn Brain Society Guidelines and Publications Committee. Update on mechanisms of the pathophysiology of neonatal encephalopathy. *Semin Fetal Neonatal Med*. 2021;26(5):101267. doi:10.1016/j.siny.2021.101267
5. Deng Q, Wu C, Liu TC, Duan R, Yang L. Exogenous lactate administration: a potential novel therapeutic approach for neonatal hypoxia-ischemia. *Exp Neurol*. 2023;367:114450. doi:10.1016/j.expneurol.2023.114450
6. Tagin MA, Woolcott CG, Vincer MJ, Whyte RK, Stinson DA. Hypothermia for neonatal hypoxic ischemic encephalopathy: an updated systematic review and meta-analysis. *Arch Pediatr Adolesc Med*. 2012;166:558-566. doi:10.1001/archpediatrics.2011.1772
7. Xu D, Vigneron D. Magnetic resonance spectroscopy imaging of the newborn brain—a technical review. *Semin Perinatol*. 2010;34:20-27. doi:10.1053/j.semperi.2009.10.003
8. Björkman ST, Miller SM, Rose SE, Burke C, Colditz PB. Seizures are associated with brain injury severity in a neonatal model of hypoxia-ischemia. *Neuroscience*. 2010;166:157-167. doi:10.1016/j.neuroscience.2009.11.067
9. Zhu W, Zhong W, Qi J, Yin P, Wang C, Chang L. Proton magnetic resonance spectroscopy in neonates with hypoxic-ischemic injury and its prognostic value. *Transl Res*. 2008;152:225-232. doi:10.1016/j.trsl.2008.09.004
10. Thayyil S, Chandrasekaran M, Taylor A, et al. Cerebral magnetic resonance biomarkers in neonatal encephalopathy: a meta-analysis. *Pediatrics*. 2010;125:e382-e395. doi:10.1542/peds.2009-1046
11. Wisnowski JL, Wu TW, Reitman AJ, et al. The effects of therapeutic hypothermia on cerebral metabolism in neonates with hypoxic-ischemic encephalopathy: an in vivo ¹H-MR spectroscopy study. *J Cereb Blood Flow Metab*. 2016;36:1075-1086. doi:10.1177/0271678X15607881
12. Thoresen M, Penrice J, Lorek A, et al. Mild hypothermia after severe transient hypoxia-ischemia ameliorates delayed cerebral energy failure in the newborn piglet. *Pediatr Res*. 1995;37:667-670. doi:10.1203/00006450-199505000-00019
13. Mikrogeorgiou A, Chen Y, Lee BS, et al. A metabolomics study of hypoxia ischemia during mouse brain development using hyperpolarized ¹³C. *Dev Neurosci*. 2020;42:49-58. doi:10.1159/000506982
14. Chen Y, Kim H, Bok R, et al. Pyruvate to lactate metabolic changes during neurodevelopment measured dynamically using hyperpolarized ¹³C imaging in juvenile murine brain. *Dev Neurosci*. 2016;38:34-40. doi:10.1159/000439271
15. Jiang J, Liang Y, Luo Q, Zhu C. Effect of mild hypothermia on brain dialysate lactate after fluid percussion brain injury in rodents. *Neurosurgery*. 2004;54:717-718. doi:10.1227/01.NEU.0000109535.58429.49
16. Rice JE, Vannucci RC, Brierley JB. The influence of immaturity on hypoxic-ischemic brain damage in the rat. *Ann Neurol*. 1981;9:131-141. doi:10.1002/ana.410090206
17. Sheldon RA, Windsor C, Lu F, Stewart NR, Jiang X, Ferriero DM. Hypothermia treatment after hypoxia-ischemia in glutathione peroxidase-1 over-expressing mice. *Dev Neurosci*. 2024;46(2):98-111. doi:10.1159/000531204
18. Liu J, Sheldon RA, Segal MR, et al. ¹H nuclear magnetic resonance brain metabolomics in neonatal mice after hypoxia-ischemia distinguished normothermic recovery from mild hypothermia recoveries. *Pediatr Res*. 2013;74:170-179. doi:10.1038/pr.2013.88
19. Patel SD, Pierce L, Ciardiello A, et al. Therapeutic hypothermia and hypoxia-ischemia in the term-equivalent neonatal rat: characterization of a translational preclinical model. *Pediatr Res*. 2015;78:264-271. doi:10.1038/pr.2015.100
20. Semple BD, Blomgren K, Gimlin K, Ferriero DM, Noble-Haeusslein LJ. Brain development in rodents and humans: identifying benchmarks of maturation and vulnerability to injury across species. *Prog Neurobiol*. 2013;106-107:1-16. doi:10.1016/j.pneurobio.2013.04.001
21. Schmidt R, Laustsen C, Dumez JN, et al. In vivo single-shot ¹³C spectroscopic imaging of hyperpolarized metabolites by spatiotemporal encoding. *J Magn Reson*. 2014;240:8-15. doi:10.1016/j.jmr.2013.12.013
22. Ádén U, Dahlberg V, Fredholm BB, Lai LJ, Chen Z, Bjelke B. MRI evaluation and functional assessment of brain injury after hypoxic ischemia in neonatal mice. *Stroke*. 2002;33:1405-1410. doi:10.1161/01.STR.0000014608.78503.DB
23. Doman SE, Girish A, Nemeth CL, et al. Early detection of hypothermic neuroprotection using T2-weighted magnetic resonance imaging in a mouse model of hypoxic ischemic encephalopathy. *Front Neurol*. 2018;9:304. doi:10.3389/fneur.2018.00304
24. Kim Y, Chen HY, Autry AW, et al. Denoising of hyperpolarized ¹³C MR images of the human brain using patch-based higher-order singular value decomposition. *Magn Reson Med*. 2021;86:2497-2511. doi:10.1002/mrm.28887
25. Penny TR, Pham Y, Sutherland AE, et al. Optimization of behavioral testing in a long-term rat model of hypoxic ischemic brain injury. *Behav Brain Res*. 2021;409:113322. doi:10.1016/j.bbr.2021.113322
26. Lueptow LM. Novel object recognition test for the investigation of learning and memory in mice. *J Vis Exp*. 2017;(126):55718. doi:10.3791/55718
27. Shi X, Bai H, Wang J, et al. Behavioral assessment of sensory, motor, emotion, and cognition in rodent models of intracerebral hemorrhage. *Front Neurol*. 2021;12:667511. doi:10.3389/fneur.2021.667511
28. Cremer JE. Substrate utilization and brain development. *J Cereb Blood Flow Metab*. 1982;2:394-407. doi:10.1038/jcbfm.1982.45
29. Vannucci RC. Experimental biology of cerebral hypoxia-ischemia: relation to perinatal brain damage. *Pediatr Res*. 1990;27:317-326. doi:10.1203/00006450-199004000-00001
30. Burnsed JC, Chavez-Valdez R, Hossain MS, et al. Hypoxia-ischemia and therapeutic hypothermia in the neonatal mouse brain—a longitudinal study. *PLoS ONE*. 2015;10(3):e0118889. doi:10.1371/journal.pone.0118889
31. Rocha-Ferreira E, Vincent A, Bright S, Peebles DM, Hristova M. The duration of hypothermia affects short-term neuroprotection in a mouse model of neonatal hypoxic ischaemic injury. *PLoS ONE*. 2018;13(7):e0199890. doi:10.1371/journal.pone.0199890
32. Wood T, Osredkar D, Puchades M, et al. Treatment temperature and insult severity influence the neuroprotective effects of therapeutic hypothermia. *Sci Rep*. 2016;6(1):23430. doi:10.1038/srep23430
33. Tatarbe M, Wisnowski JL, Geyer E, et al. Cerebral glucose concentration in neonatal hypoxic-ischemic encephalopathy during therapeutic hypothermia. *J Pediatr*. 2023;261:113560. doi:10.1016/j.jpeds.2023.113560

34. Piñeiro-Ramos JD, Núñez-Ramiro A, Llorens-Salvador R, et al. Metabolic phenotypes of hypoxic-ischemic encephalopathy with normal vs. pathologic magnetic resonance imaging outcomes. *Metabolites*. 2020;10(3):109. doi:[10.3390/metabo10030109](https://doi.org/10.3390/metabo10030109)
35. Sánchez-Abarca LI, Tabernero A, Medina JM. Oligodendrocytes use lactate as a source of energy and as a precursor of lipids. *Glia*. 2001;36:321-329. doi:[10.1002/glia.1119](https://doi.org/10.1002/glia.1119)
36. Vicario C, Tabernero A, Medina JM. Regulation of lactate metabolism by albumin in rat neurons and astrocytes from primary culture. *Pediatr Res*. 1993;34:709-715. doi:[10.1203/00006450-199312000-00002](https://doi.org/10.1203/00006450-199312000-00002)
37. Cremer JE, Cunningham VJ, Pardridge WM, Braun LD, Oldendorf WH. Kinetics of blood-brain barrier transport of pyruvate, lactate and glucose in suckling, weanling and adult rats. *J Neurochem*. 1979;33:439-445. doi:[10.1111/j.1471-4159.1979.tb05173.x](https://doi.org/10.1111/j.1471-4159.1979.tb05173.x)
38. Pellerin L, Pellegrini G, Martin JL, Magistretti PJ. Expression of monocarboxylate transporter mRNAs in mouse brain: support for a distinct role of lactate as an energy substrate for the neonatal vs. adult brain. *Proc Natl Acad Sci U S A*. 1998;95:3990-3995. doi:[10.1073/pnas.95.7.3990](https://doi.org/10.1073/pnas.95.7.3990)
39. Lally PJ, Montaldo P, Oliveira V, et al. Magnetic resonance spectroscopy assessment of brain injury after moderate hypothermia in neonatal encephalopathy: a prospective multicentre cohort study. *Lancet Neurol*. 2019;18:35-45. doi:[10.1016/S1474-4422\(18\)30325-9](https://doi.org/10.1016/S1474-4422(18)30325-9)
40. Ancora G, Testa C, Grandi S, et al. Prognostic value of brain proton MR spectroscopy and diffusion tensor imaging in newborns with hypoxic-ischemic encephalopathy treated by brain cooling. *Neuroradiology*. 2013;55:1017-1025. doi:[10.1007/s00234-013-1202-5](https://doi.org/10.1007/s00234-013-1202-5)
41. Chung BT, Chen HY, Gordon J, et al. First hyperpolarized [^{13}C] pyruvate MR studies of human brain metabolism. *J Magn Reson*. 2019;309:106617. doi:[10.1016/j.jmr.2019.106617](https://doi.org/10.1016/j.jmr.2019.106617)
42. Park JM, Josan S, Grafendorfer T, et al. Measuring mitochondrial metabolism in rat brain in vivo using MR spectroscopy of hyperpolarized [^{13}C] pyruvate. *NMR Biomed*. 2013;26:1197-1203. doi:[10.1002/nbm.2935](https://doi.org/10.1002/nbm.2935)

How to cite this article: Liu X, Manninen T, Capper AM, et al. Brain metabolism after therapeutic hypothermia for murine hypoxia-ischemia using hyperpolarized [^{13}C] pyruvate magnetic resonance spectroscopy. *NMR in Biomedicine*. 2024;37(10):e5196. doi:[10.1002/nbm.5196](https://doi.org/10.1002/nbm.5196)